Characterization of the Oxidation Products of Styryl-Substituted Terthiophenes and Sexithiophenes Using Electronic Absorption Spectroscopy and Time-Dependent DFT

Tracey M. Clarke,[†] Keith C. Gordon,*[,†] David L. Officer,[‡] and Daina K. Grant[‡,§]

Department of Chemistry, University of Otago, PO Box 56, Dunedin, New Zealand and Nanomaterials Research Centre, IFS - Chemistry, Massey University, Palmerston North, New Zealand, and New Zealand Institute for Crop & Food Research Ltd., Private Bag 11600, Palmerston North, New Zealand

Received: June 25, 2004; In Final Form: October 26, 2004

The electronic absorption spectra of a series of alkoxy-styryl substituted terthiophenes, their corresponding sexithiophenes, and the oxidation products of both have been measured. The terthiophenes studied σ-dimerize to sexithiophenes during the oxidation process and there is clear evidence of sexithiophene radical cations, dications, and π-dimers in the electronic absorption spectra. The oxidation of concentrated solutions produces predominantly π-dimer bands, as expected. The absorption spectrum of the styryl-functionalized sexithiophene dication without alkoxy substitution closely resembles that of unsubstituted sexithiophene, while alkoxy substitution induces changes in the wavelength of the dication band maximum and the overall band shape. Time-dependent density functional theory (TDDFT) calculations have shown that styryl-based molecular orbitals are important in the transitions of the neutral molecules as well as the charged species, the dication in particular. Kinetics analyses confirm the stabilization effect induced by the alkoxy substituents. The presence of a reversible π-dimer equilibrium was verified by cyclic voltammetry. It is clear from the experimental observations and the theoretical calculations that both the styryl and alkoxy groups are influencing the electronic properties of this class of molecules.

I. Introduction

Conjugated polymers, such as polythiophenes, offer several potential opportunities for utilization in plastic electronics applications such as field-effect transistors,[1] OLEDs,[2] and plastic photovoltaic cells.[3,4] Their suitability for these applications results from their unique electronic and optoelectronic properties. When polythiophene (a nondegenerate polymer) is oxidized, the resultant radical cation, a positive polaron, is defined by both the charged excitation and the structural defect that it induces (a domain of quinoid-type bond sequence).[5] These charged defects are localized over several monomer units. If further oxidation is able to produce the dication, then a second polaron forms and two of these species can combine to form a spinless bipolaron, a process dependent on the length of the oligomer.[6−9] There remains some uncertainty over which type of charged defect, polarons or bipolarons, is principally responsible for the conductivity observed in nondegenerate conjugated polymers. In addition, the precise mechanism of conduction is still unclear, especially the path of the charge carriers through the polymer. An increased understanding of the conduction mechanism should lead to a more rational design of polymers and therefore enhance the efficiency of the resultant plastic electronic devices.

Investigations of the oxidation behavior of well-defined oligothiophenes have proved valuable in that oligothiophene radical cations and dications provide suitable models for the polaron and bipolaron states of polythiophenes. Electronic absorption spectroscopy is an important method for following oligothiophene oxidation reactions and characterizing the nature of the end products. However, adequate experimental electronic absorption spectra can be difficult to obtain for the radical cations of short unsubstituted oligothiophenes, such as terthiophene, because of their short lifetimes.[10] For example, terthiophene radical cation species are so reactive that they exist on the microsecond time scale.[11,12] Time-resolved methods such as laser flash photolysis,[11,13] pulse radiolysis,[14] and a recent picosecond time-resolved spectroscopic study[12] have provided the absorption spectrum of the unsubstituted terthiophene radical cation. This species rapidly dimerizes to form sexithiophene.[15,16] Sexithiophene radical cations are significantly more stable than their terthiophene counterparts and sexithiophene dications are often observed if the oxidation reaction is continued. In attempts to study the terthiophene radical cation, and not its dimerization products, several strategies have been employed. The use of α,α'-end caps[17−20] and high dilution conditions[15] to prevent dimerization are tactics that have proven successful.

Many studies have been performed on the electronic absorption properties of terthiophene and sexithiophene radical cations.[11,14,21−25] Two strong bands are observed for radical cations, one in the visible region and the other in the near-infrared (NIR). These bands appear at 550 and 850 nm for the unsubstituted terthiophene radical cation[11,12,22] and at 780 and 1476 nm for the radical cation of unsubstituted sexithiophene.[15] These bands have been assigned to transitions between the singly occupied MO (SOMO) and LUMO and between the doubly occupied HOMO-1 and SOMO, respectively. Small sidebands at higher energy are also often observed, depending upon the oxidation conditions, and are often attributed to either vibronic transitions[21] or to π-dimers.[17] Substitution, with either α,α'-end caps or solubilizing β-groups, usually results in red-shifting of the bands and in general such terthiophene radical cation bands are measured at 550−650 nm and 850−1150 nm[13,17,18,23,24] while the corresponding sexithiophene radical cation bands are observed at 760−860 nm and 1460−1700 nm.[9,16,18,20,25] Olig-

* Corresponding author. E-mail: kgordon@alkali.otago.ac.nz.
[†] University of Otago.
[‡] Massey University.
[§] Crop & Food Ltd.

10.1021/jp0404551 CCC: $30.25
Published on Web 02/15/2005

othiophene dications, in contrast, present only one strong band, intermediate in energy between the two radical cation transitions, assigned to the HOMO−LUMO transition. Sexithiophene, the shortest unsubstituted oligothiophene to show evidence of dication formation, has its dication transition at 1000 nm with a vibronic[19] shoulder at 912 nm.[15] The position of the main band alters to some extent with substitution and in general appears around 950−1100 nm.[9,16,19,20,25]

π-Dimers have also been observed in the electronic absorption spectra of oxidized oligothiophenes.[7,19,20,23,24,26,27] These result from a face-to-face π interaction of two separate radical cations, resulting in a pairing of the unpaired electrons' spins. π-Dimers are favored in acetonitrile as opposed to dichloromethane:[19,23,24] the greater polarity of acetonitrile is able to stabilize the interaction. Other factors that promote the formation of π-dimers are high oligomer concentrations[28] and low temperatures.[17] The presence of π-dimers has therefore often been demonstrated through variable-temperature absorption spectroscopy,[7,23] where the two radical cation bands decay as the temperature decreases and three new bands appear, two blue-shifted with respect to the parent radical cation bands and the other a charge-transfer band at low energy. Variable-temperature ESR has also provided evidence of π-dimers; a diamagnetic species forms at low temperatures when oligothiophene radical cation samples are cooled.[10,23] The X-ray structure of the 3′,4′-dibutyl-5,5″-diphenyl-terthiophene radical cation shows that π-stacking occurs in crystals.[24]

The purpose of this work is to examine the oxidation processes, and thus identify the nature of the charged species that form, of a series of styryl-substituted terthiophenes, 3′-[1*E*-2-(3-R_1,4-R_2-phenyl) ethenyl]-2,2′:5′,2″-terthiophene, and their corresponding sexithiophenes via electronic absorption spectroscopy. The structures of the compounds to be studied are depicted in Figure 1. Two oxidation conditions were examined, copper perchlorate ($Cu(ClO_4)_2$) in acetonitrile and iron chloride ($FeCl_3$) in dichloromethane, since the probabilty of π-dimer formation is greater in acetonitrile than in dichloromethane.[15,18] The oxidations were terminated with hydrazine.[9,28] To further investigate the π-dimer equilibria that are present for the compounds studied in this work, two different oligothiophene concentrations were studied. Time-dependent DFT calculations were also performed to investigate the electronic processes involved in the transitions. The spectral changes were studied in a kinetics analysis to assess the reactivities of the oxidation products.

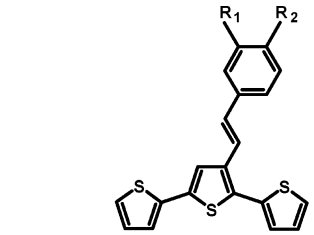

I: R_1 = -H, R_2 = -H
II: R_1 = -H, R_2 = -OCH_3
III: R_1 = -OCH_3, R_2 = -OCH_3
V: R_1 = -OCH_3, R_2 = -$O(C_2H_4O)_3CH_3$

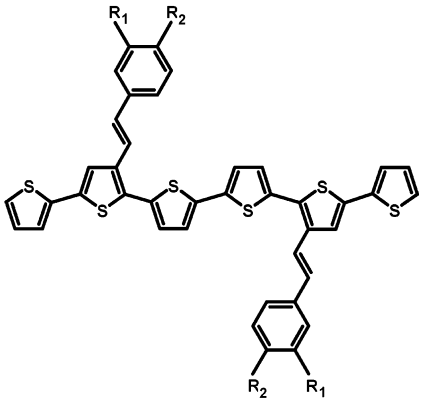

IV: R_1 = -OCH_3, R_2 = -OCH_3
VI: R_1 = -OCH_3, R_2 = -$O(C_2H_4O)_3CH_3$

Figure 1. The chemical structures of compounds **I**−**VI**.

II. Experimental Section

The synthesis and purification methods of the compounds studied are described elsewhere.[29,30]

Chemical oxidations were performed using $1.0-4.0 \times 10^{-5}$ mol L^{-1} and $1.0-3.0 \times 10^{-4}$ mol L^{-1} oligothiophene solutions, prepared with spectrophotometric grade acetonitrile. Aliquots (5−20 μL) of oxidant, a solution of 8×10^{-4} mol L^{-1} copper perchlorate in acetonitrile ($Cu(ClO_4)_2/CH_3CN$), were added until a maximum of three equivalents was reached. The two sexithiophenes, **IV** and **VI** (1.5×10^{-5} mol L^{-1}), were also oxidized using a solution of anhydrous ferric chloride in dichloromethane (maximum concentration 2×10^{-4} mol L^{-1}). Reduction of each final oxidation product was achieved by adding one drop of a 2% hydrazine aqueous solution.

Quartz cells of two different path lengths were used: 10 mm for the 10^{-5} mol L^{-1} solutions and 1 mm for the 10^{-4} mol L^{-1} solutions. Electronic absorption spectra were measured at room temperature from 200 to 2000 nm on a Varian Cary 500 Scan UV-Vis-NIR Spectrophotometer using Cary WinUV Scan Application software. Spectra were analyzed using GRAMS 5.0 (Galactic Industries). Kinetics analyses were performed on thermostated solutions (25 °C) which were allowed to equilibrate for 10 min prior to oxidation. The absorbance of each freshly oxidized solution was measured over a 90-min period at a series of wavelengths, each corresponding to the absorption maxima of the required species.

Cyclic voltammograms were measured at room temperature using $10^{-4}-10^{-3}$ mol L^{-1} solutions. All solutions were prepared in 0.1 mol L^{-1} tetrabutylammonium perchlorate (TBAP) in acetonitrile and degassed with nitrogen for 5 min prior to measurement. The data were acquired at scan speeds of 0.1−20 V s^{-1} using an AdInstruments Powerlab 4sp potentiostat controlled by a PC running Powerlab EChem software. The electrochemical cell consisted of a 1.0-mm diameter platinum working electrode embedded in a Kel-F cylinder with a platinum auxiliary electrode and a saturated potassium chloride calomel reference electrode (SCE). The decamethylferrocenium/decamethylferrocene ($Me_{10}Fc^{+/0}$) redox couple was used as an internal standard.[31]

Vertical electronic excitation energies were calculated for unsubstituted sexithiophene, $(\mathbf{I})_2$ and $(\mathbf{II})_2$ and their respective radical cations and dications using time-dependent density functional theory (TDDFT). This was accomplished using the B3LYP/6-31G(d) method with the Gaussian 03 program.[32] A spin-unrestricted wave function was used for the radical cations (UB3LYP). Geometry optimizations were performed first, with C_2 symmetry imposed onto the $(\mathbf{I})_2$ and $(\mathbf{II})_2$ systems and their charged species (because of the large number of basis functions involved in the calculation).

TABLE 1: Electronic Absorption Data and Assignments of the Chemical Oxidations of Compounds I−VI (10^{-5} mol L^{-1})[a]

compound	neutral		radical cation	π-dimer			dication			reduced	
				$Cu(ClO_4)_2$/ CH_3CN							
I	310		1466	806	1170	695[b]	984	890[b]		438	317
II	321		1525[b]	815[b]	1192	724	965[b]	889	527	435	326
III	329			820[b]	1205	724		886	545	441	334
IV	439	334	1580[b]	820[b]	1218	725		887	553	437	333
V	329			825[b]	1217	748		894	551	436	333
VI	444	334		820[b]	1223	733		895	547	437	334
				$FeCl_3/CH_2Cl_2$							
IV	444	336	1720	840							
VI	446	335	1705	839	1168	694					

[a] Band positions are in nanometers. [b] Shoulder.

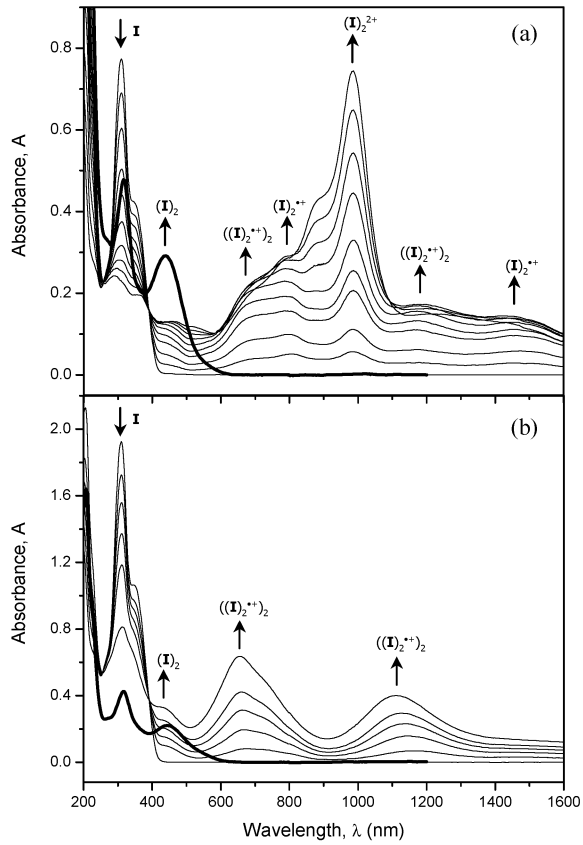

Figure 2. Evolution of the electronic absorption spectra during the chemical oxidations of 10^{-5} mol L^{-1} (a) and 10^{-4} mol L^{-1} (b) **I** using an 8×10^{-4} mol L^{-1} solution of $Cu(ClO_4)_2$ in acetonitrile. The two spectra shown in bold correspond to the reduction of the end oxidation product with aqueous hydrazine. The terminology used in the figure is defined as follows: **I** = neutral terthiophene; $(\mathbf{I})_2$ = neutral sexithiophene; $(\mathbf{I})_2^{\bullet+}$ = sexithiophene radical cation; $(\mathbf{I})_2^{2+}$ = sexithiophene dication; $((\mathbf{I})_2^{\bullet+})_2$ = sexithiophene π-dimer.

III. Results and Discussion

III.a. Electronic Absorption Spectroscopy. The electronic absorption data obtained for the oxidation of the 10^{-5} mol L^{-1} oligothiophene solutions are presented in Table 1.

3′-[1*E*-2-(Phenyl)ethenyl]-2,2′:5′,2″-terthiophene (I). The absorption spectra of the oxidation of 10^{-5} mol L^{-1} **I** with $Cu(ClO_4)_2$ show the growth of several bands in the visible and NIR regions with the concurrent decay of the neutral terthiophene band at 310 nm (Figure 2a). The isosbestic point at 389 nm suggests a clean interconversion between the neutral species and its oxidation products.[17] However, reduction of the final oxidized species with hydrazine did not regenerate the original terthiophene spectrum. Instead, two bands were observed at 438 and 317 nm. This is consistent with a neutral styryl-substituted sexithiophene (vide infra), indicating that the species formed in the oxidation reaction are that of the σ-dimerized terthiophene and not the terthiophene itself. The σ-dimerization process of the terthiophene radical cation is too fast to be observed on the time scale of these experiments and no spectroscopic evidence of any terthiophene charged species is observed in this work: this correlates with the well-known instability of terthiophene radical cations lacking α end-caps.[28] The shoulder at 440 nm observed during the oxidation process was therefore assigned to the neutral sexithiophene species.

Of the several new bands that form during the oxidation, sexithiophene radical cation $(\mathbf{I})_2^{\bullet+}$ bands are observed at 1466 and 806 nm, at similar wavelengths to those of unsubstituted sexithiophene (1476 and 780 nm).[15] The 806-nm band has a shoulder at 695 nm and another band is apparent at 1170 nm. The wavelengths of these bands are consistent with π-dimer, $((\mathbf{I})_2^{\bullet+})_2$, formation:[25] they are blue-shifted with respect to the parent radical cation bands by 0.21 eV for the NIR band and 0.24 eV for the visible band. These separations are similar to that seen for the corresponding bands of an end-capped sexithiophene with β-substituted methoxy groups (0.25 and 0.31 eV, respectively),[20] which were also assigned to π-dimers. Fichou's[15] unsubstituted sexithiophene radical cation spectrum was reinterpreted by Bäuerle et al.[17] to include π-dimer formation and the separations observed are 0.23 and 0.14 eV. It is unlikely that the 695-nm shoulder and 1170-nm band are due to vibronic transitions because the separation from the main radical cation bands is too large, about 1700 cm^{-1}.[33] The proposal that $((\mathbf{I})_2^{\bullet+})_2$ is formed in acetonitrile is supported by the observation that for 3′,4′-dibutyl-5,5″-diphenyl-terthiophene the equilibrium constant of π-dimerization is 3 orders of magnitude higher in acetonitrile (0.6) than in dichloromethane (3×10^{-4});[24] this is due to the more polar acetonitrile's ability to reduce the Coulombic interactions that occur between the two radical cations as they π-dimerize. In addition, it has been established that longer oligothiophenes π-dimerize more readily, even at room temperature.[17,20,26] It is thus expected that the oxidation of a sexithiophene derivative in acetonitrile will produce evidence of π-dimerization, even at room temperature, as shown in the absorption spectra of oxidized **I** (Figure 2a). The low-energy charge-transfer band of the π-dimer cannot be observed as its oscillator strength is generally lower than that of the two higher energy bands and the several acetonitrile bands at 1600−2000 nm are thus probably obscuring it.

The band at 984 nm has been assigned to the sexithiophene dication, $(\mathbf{I})_2^{2+}$. It appears very early in the oxidation process, concurrent with the radical cation peaks, before the neutral band has disappeared and before one equivalent of oxidant is reached.

This may imply the presence of a disproportionation reaction,[9] in which two radical cations react to produce a neutral molecule and a dication. Alternatively, it may simply mean that dication formation is a highly facile reaction. As the oxidation continues, this band grows to dominate the spectrum and a shoulder at 890 nm, often assigned to vibronic coupling,[21] becomes apparent. Use of excess oxidant leads to direct formation of $(\mathbf{I})_2^{2+}$. The band is very intense, significantly more so than the bands of the radical cation. This greater intensity of the dication band has been observed in the oxidation of other oligothiophenes.[34]

To investigate the π-dimer phenomenon further, higher concentrations of **I** were examined (the stability of the radical cation is not high enough to enable variable temperature experiments).[7] The oxidation of 10^{-4} mol L^{-1} **I** with $Cu(ClO_4)_2$ produced bands at similar wavelengths to that observed in the early oxidation stage of the dilute (10^{-5} mol L^{-1}) **I** solution, but the intensity pattern is different (Figure 2b). The two main bands are located at 1164 and 678 nm, with shoulders at 1450 nm (barely discernible) and 730 and 810 nm, respectively. On the basis of the assignments made for the dilute **I** experiment, the 1450- and 810-nm shoulders are due to $(\mathbf{I})_2^{\bullet+}$, while the 1164- and 678-nm bands are π-dimer transitions. The 730-nm band is probably due to vibronic coupling. The relegation of the radical cation bands to shoulders while the π-dimer bands now dominate the spectrum reflects the fact that π-dimer formation is more favorable at higher oligothiophene concentrations.[28] Further oxidation causes a small hypsochromic drift: the π-dimer bands shift from their original positions of 1164 and 678 nm to 1113 and 657 nm, respectively. This small shift ($\sim$0.05 eV) has also been observed during the oxidation of a neutral substituted duodecithiophene to its radical cation.[9] Neutral σ-dimers still result from NH_2NH_2 reduction. Reaction of the concentrated **I** solution (10^{-4} mol L^{-1}) with excess oxidant (0.1 mol L^{-1}) produces the $(\mathbf{I})_2^{2+}$ band, which rapidly decays with time while another band at 751 nm increases in intensity. The identity of this 751-nm band is not certain, but reduction still produces the two-band feature (437 and 317 nm) indicative of the neutral sexithiophene.

It therefore appears that the fate of $(\mathbf{I})_2^{\bullet+}$ varies depending on the concentration of **I** used. Dilute **I** allows facile production of $(\mathbf{I})_2^{2+}$, simultaneously with the radical cation. However, in the 10^{-4} mol L^{-1} **I** solution, formation of the dication requires an excess of oxidant and it is unstable under these conditions. Instead, π-dimer formation seems to be the favored pathway at higher **I** concentrations.

3′-[1*E*-2-(4-Methoxy-phenyl)ethenyl]-2,2′:5′,2″-terthiophene (II). The oxidation of 10^{-5} mol L^{-1} **II** also produces evidence of sexithiophene species, as shown in Figure 3. In particular, reduction of the final oxidation product generates the two distinctive neutral sexithiophene bands at 435 and 326 nm. The 435-nm band is apparent as a shoulder during the oxidation process. The first stage in the oxidation involves two weak, broad bands at 1192 and 724 nm, each with a shoulder located at 1525 and 815 nm, respectively. These shoulders can be assigned to the sexithiophene radical cation, $(\mathbf{II})_2^{\bullet+}$, while the main bands are likely due to π-dimers. In contrast to **I**, the π-dimer bands are consistently of higher intensity than the radical cation bands. π-Dimer formation, therefore, appears to be more favorable for **II** than for **I**.

As the oxidation of **II** progresses, a band consistent with the dication, $(\mathbf{II})_2^{2+}$, appears at 889 nm with a shoulder at $\sim$965 nm. There is also a higher energy band at 527 nm, which has been observed in other sexithiophene dication absorption spectra[16,35] and assigned to the normally forbidden bipolaron

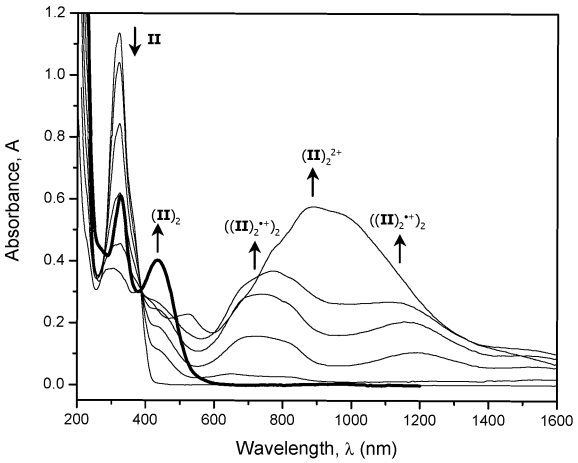

Figure 3. Evolution of the electronic absorption spectra during the chemical oxidation of 10^{-5} mol L^{-1} **II** using an 8×10^{-4} mol L^{-1} solution of $Cu(ClO_4)_2$ in acetonitrile. The spectrum shown in bold corresponds to the reduction of the end oxidation product with aqueous hydrazine.

transition between the HOMO and the LUMO+1.[9] Its appearance in a spectrum generally indicates lower symmetry. The principal dication band, however, is interesting in that its structure is very different to that of both $(\mathbf{I})_2^{2+}$ and unsubstituted sexithiophene. The intensities of the main band and the shoulder have effectively switched: the absorption maximum is blue-shifted and the transition close to 1000 nm has been relegated to a shoulder. A possible explanation for this behavior is discussed later on the basis of TDDFT calculations (section III.d).

The oxidation of 10^{-4} mol L^{-1} **II** produces π-dimer bands at 1191 and 717 nm, which shift to 1176 and 698 nm as the reaction proceeds (Figure 1S). This is analogous behavior to that of **I** under similar experimental conditions. A shoulder is also visible at $\sim$820 nm (assigned to the sexithiophene radical cation).

3′-[1*E*-2-(3,4-Dimethoxy-phenyl)ethenyl]-2,2′:5′,2″-terthiophene (III). The oxidation of **III** provides very similar absorption spectra to that of **II**, in terms of the band positions and the overall pattern produced upon oxidation. Once again, σ-dimerization of terthiophene radical cations has occurred to form sexithiophene oxidation products: reduction produces two bands at 441 and 334 nm (Figure 2S). The π-dimer bands are the principal ones at the early stage of oxidation, situated at 1205 and 724 nm. One of the radical cation bands is visible as a shoulder at 820 nm, but the second band cannot be discerned. The oxidation progresses to reveal the $(\mathbf{III})_2^{2+}$ band at 886 nm. The lower energy band seen at $\sim$965 nm in the spectrum of **II** is not evident here. However, there is a broad shoulder at approximately 1150 nm, but whether this is the continued presence of the 1205-nm π-dimer band or another dication transition is unclear. The $(\mathbf{III})_2^{\bullet+}$ and π-dimer bands are red-shifted with respect to the corresponding bands of **I**, the result of the electron-donating methoxy groups stabilizing the radical cation.[20]

The higher concentration of **III** (10^{-4} mol L^{-1}) was also oxidized, again exhibiting comparable behavior to **II** with π-dimer bands initially at 1206 and 725 nm blue-shifting to 1170 and 701 nm (Figure 3S). The magnitude of the shift is similar to that observed for **II**. As was the case with **II**, no dication band is evident when the higher oligothiophene concentration is used, although a weak $(\mathbf{III})_2^{\bullet+}$ shoulder is present at 830 nm.

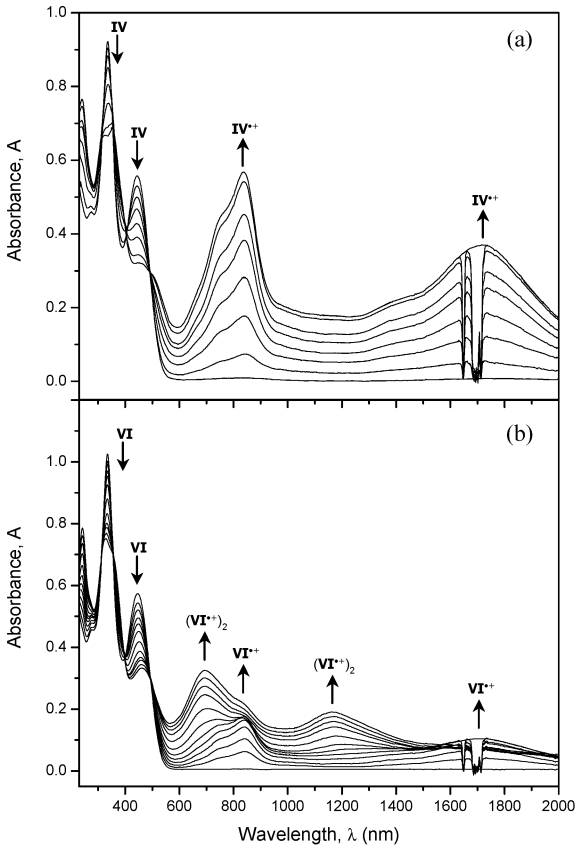

Figure 4. Evolution of the electronic absorption spectra during the chemical oxidations of 10^{-5} mol L^{-1} **IV** (a) and 10^{-5} mol L^{-1} **VI** (b) using a solution of $FeCl_3$ in dichloromethane (maximum concentration 2×10^{-4} mol L^{-1}). The distortion at 1630−1730 nm is a result of the solvent subtraction.

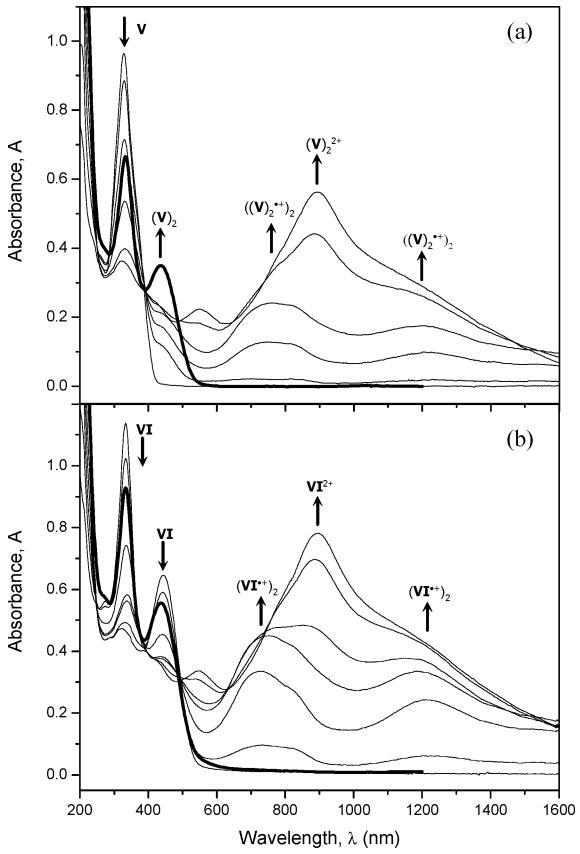

Figure 5. Comparison of the electronic absorption spectra measured during the chemical oxidations of 10^{-5} mol L^{-1} **V** (a) and 10^{-5} mol L^{-1} **VI** (b) using an 8×10^{-4} mol L^{-1} solution of $Cu(ClO_4)_2$ in acetonitrile. The two spectra shown in bold correspond to the reduction of the end oxidation product with aqueous hydrazine.

4′,3‴′-Bis-[1*E*-2-(3,4-dimethoxy-phenyl)ethenyl]-2,2′:5′,2″:5″,2‴:5‴,2⁗:5⁗ ″,2⁗′-sexithiophene (IV). Compound **IV**, the neutral dimer of **III**, consists solely of the head-to-head isomer, as shown by NMR studies.[30,36] The peaks of neutral **IV** are located at 439 and 334 nm (Figure 4S), identical to the band positions of neutral σ-dimerized **III** (within the experimental uncertainty of the spectrometer). The oxidation of **IV** with $Cu(ClO_4)_2$ produces π-dimer bands at 1218 and 725 nm, with radical cation shoulders at ∼1580 and 820 nm. Further oxidation produces the broad and intense 887-nm dication band, along with the weaker 553-nm band. Reduction regenerates neutral **IV**, with bands at 437 and 333 nm, indicating that the sexithiophene charged species are relatively stable and are not undergoing oligomerization. The similarities between this oxidation behavior and that observed for its monomer, **III**, verify that the oxidation of **III** does indeed produce sexithiophene products.

Using higher concentrations of **IV** reproduces the π-dimer band positions (Figure 5S). The blue-shifting of the π-dimer bands is observed as for the preceding terthiophene oxidations when high substrate concentrations are used. Dication formation is not observed.

To identify the band positions of $\mathbf{IV}^{\bullet+}$ more clearly, the oxidation of **IV** was also performed using $FeCl_3/CH_2Cl_2$, π-dimer formation being less favorable in dichloromethane. The bands of the neutral species in CH_2Cl_2 are very slightly red-shifted compared to that observed in acetonitrile and are located at 444 and 336 nm (Figure 4a). The oxidation shows an isosbestic point at 492 nm, reflecting the clean formation of the radical cation. The two principal $\mathbf{IV}^{\bullet+}$ bands are positioned at 1720 and 840 nm. Shoulders are apparent on the high-energy side of each, at 1400 and 755 nm. Unless solvatochromic effects are active here, it is likely that these shoulders are due to vibrational transitions (rather than π-dimers), being separated by 0.17 eV (1330 cm^{-1}) and 0.16 eV (1340 cm^{-1}), respectively, from the main radical cation bands. These radical cation bands are appreciably more intense than the corresponding bands in acetonitrile. In addition, they show significant red-shifts with respect to the corresponding bands of the unsubstituted sexithiophene radical cation of 0.11 eV for the visible band and 0.12 eV for the NIR band (in the same solvent).[15] This implies a considerable stabilization effect induced by the alkoxy-styryl substituents. No $\mathbf{IV}^{2+}$ formation is observed in dichloromethane.

3′-[1*E*-2-(3-Methoxy-4{methoxy-ethoxy-ethoxy-ethoxy}-phenyl)ethenyl]-2,2′:5′,2″-terthiophene (V). The oxidation of **V**, shown in Figure 5a, produces very similar behavior to the other terthiophene oxidations, with sexithiophene π-dimer bands forming at 1217 and 748 nm and a radical cation shoulder clearly visible at 825 nm. The second radical cation band is obviously of too low an oscillator strength to be readily apparent. These band positions continue the trend of a bathochromic shift across the compound series: the NIR π-dimer band of **I**, for example, is located at 1170 nm, which shifts to 1192, 1205, and then 1217 nm with increasing alkoxy substitution. The second π-dimer band also exhibits this trend (695, 724, 724, and 748 nm), as does the radical cation transition in the visible region (806, 815, 818, and 825 nm). The NIR radical cation band is generally not clear enough to enable accurate determination of the band position. Interestingly, the position of the $(\mathbf{V})_2^{2+}$ band, observed at 894 nm, does not show this trend. All four

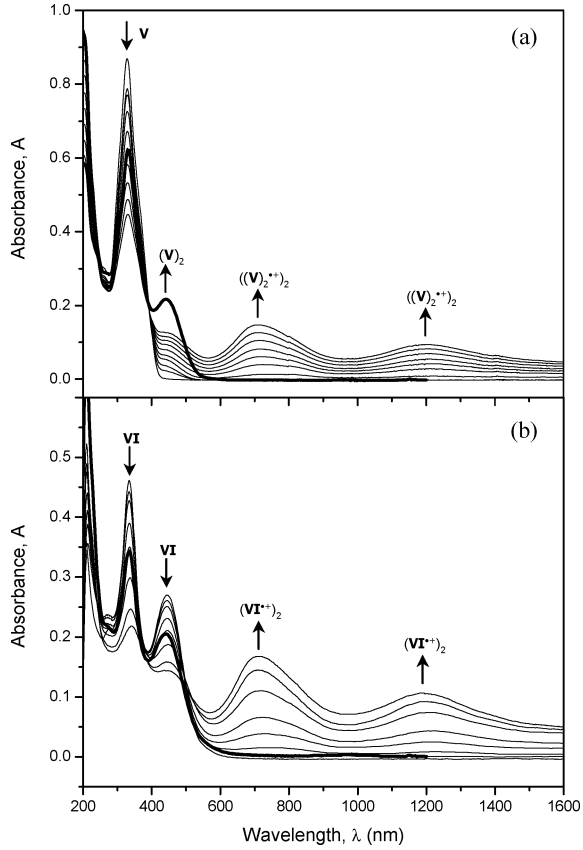

Figure 6. Comparison of the electronic absorption spectra measured during the chemical oxidations of 10^{-4} mol L^{-1} **V** (a) and 10^{-4} mol L^{-1} **VI** (b) using an 8×10^{-4} mol L^{-1} solution of $Cu(ClO_4)_2$ in acetonitrile. The two spectra shown in bold correspond to the reduction of the end oxidation product with aqueous hydrazine.

terthiophenes show this band at approximately the same wavelength (890, 889, 886, and 894 nm). Reduction of either oxidized **V** species, the π-dimer or the dication, generates the neutral sexithiophene with bands at 436 and 333 nm.

Oxidation of more concentrated **V** (10^{-4} mol L^{-1}) generates the two π-dimer bands that hypsochromically drift from 1217 and 732 nm to 1204 and 711 nm as the reaction proceeds (Figure 6a). The shoulder evident at 820 nm, attributed to $(\mathbf{V})_2^{\bullet+}$, does not appear to shift. This, as previously discussed, is similar behavior to that observed for all preceding compounds. In addition, no $(\mathbf{V})_2^{2+}$ formation is apparent when the higher substrate concentration is used, also analogous to the previous compounds.

4′,3‴′-Bis-[1*E*-2-(3-methoxy-4-{methoxy-ethoxy-ethoxy}-phenyl)ethenyl]-2,2′:5′,2″:5″,2‴:5‴,2⁗:5⁗,2⁗′-sexithiophene (VI). Compound **VI**, the neutral dimer of **V**, also consists of exclusively the head-to-head regioisomer. The bands of the neutral species are at 444 and 334 nm in acetonitrile (Figure 5b). Oxidation produces π-dimer bands at 1223 and 733 nm and a radical cation shoulder at 820 nm, comparable to that observed for its monomer, **V**. The sexithiophene dication, with its band maximum at 895 nm along with the weaker band at 547 nm, is formed upon further oxidation. NH_2NH_2 reduction regenerates neutral **VI**. The use of more concentrated **VI** reveals only π-dimer bands and their blue-shifts from 1214 and 730 nm to 1191 and 712 nm (Figure 6b).

As was the case with **IV**, the oxidation of **VI** was also accomplished using $FeCl_3/CH_2Cl_2$. The absorption spectra of this oxidation are shown in Figure 4b. The neutral bands of **VI** in this solvent are located at 446 and 335 nm. The initial stage of oxidation is equivalent to that of **IV**, with radical cation bands appearing at 1705 and 839 nm, with the latter band exhibiting a shoulder at 750 nm. Further addition of oxidant leads to decay of the 1705-nm band, growth of π-dimer bands, and the decline of the 839-nm band to a shoulder, features not observed in the $FeCl_3$ oxidation of **IV**. The π-dimer bands appear at 1168 and 694 nm, separated from the original radical cation bands by 0.33 and 0.31 eV, respectively. This is a larger separation than that observed in acetonitrile. The formation of these π-dimer bands increase the probability that the 750-nm shoulder (also observed in the oxidation of **IV**, at 755 nm) is attributable to a vibrational transition of the main radical cation band, as previously discussed. The presence of π-dimers may be a result of the longer alkoxy chain providing further stabilization of the radical cation, in comparison to $\mathbf{IV}^{\bullet+}$, thus allowing π-dimerization in this solvent.

III.b. Kinetics Analysis. We have investigated the kinetic behavior of the observed spectral changes for several of the compounds studied here (**I**, **IV**, and **VI**). The change in absorbance over time was measured at various wavelengths, each representing an absorption band maximum for the pertinent species: the neutral species, the σ-dimer of the terthiophene, and the sexithiophene radical cation and dication. The oxidation process involves several steps and possible pathways, some of which are reversible. These factors lead to very complicated kinetics and thus a relatively qualitative approach has been taken. In addition, the extinction coefficients (ϵ) of the **I** σ-dimer and each sexithiophene dication were estimated to convert the absorbance measurements to concentrations such that rate data could be derived. This was done by oxidizing each compound with an excess of $Cu(ClO_4)_2$ (then reducing the products with hydrazine) and converting the maximum absorbance of the relevant peak to the extinction coefficient of that species, assuming reaction completion at each stage. Clearly this method cannot be applied to the radical cation as it is a true intermediate and thus its extinction coefficient cannot be estimated with any accuracy. However, despite the complexities inherent in the oxidation process and the need to estimate extinction coefficients, several key kinetic features have been discovered.

The terthiophene species that was investigated in this manner (**I**) shows evidence of the formation of sexithiophene species within one second of the oxidation process commencing. No terthiophene charged intermediates are observed at all, consistent with the very short lifetime expected for a terthiophene radical cation with no α end-caps (μs time scale).[12] The changes in the absorbance over time for each **I** species are illustrated in Figure 7.

In **I**, the concentrations of both the substrate and the oxidant were varied to establish the orders with respect to each reactant. Only the initial rates were examined because of the complicated nature of the oxidation process, and these are shown in Table 2. For the alteration of the oxidant concentration, 1, 3, and 10 equivalents of $Cu(ClO_4)_2$ were added. The initial rates indicate that the formation of $(\mathbf{I})_2$ and its radical cation and dication are all first-order with respect to $[Cu^{2+}]$. The decay of neutral **I** is also dependent upon $[Cu^{2+}]$: within experimental uncertainty, the results indicate an order of one with respect to $[Cu^{2+}]$. The formation of $(\mathbf{I})_2^{\bullet+}$ and $(\mathbf{I})_2^{2+}$ both appear to be second-order with respect to [**I**]. In turn, this implies that the radical cation and dication formation reactions are third-order overall.

The formation of $(\mathbf{I})_2^{2+}$ when only one equivalent of oxidant has been added to the monomer solution suggests that dication formation from the radical cation is a highly facile process: dication formation is occurring simultaneously with the $(\mathbf{I})_2 \rightarrow$

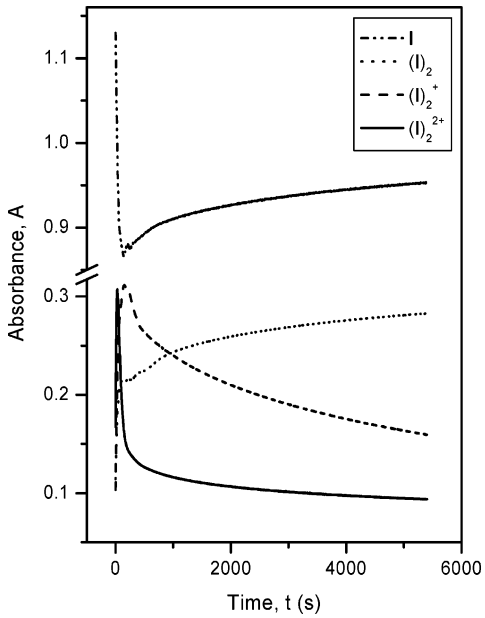

Figure 7. The absorbance versus time curves measured during the oxidation of **I** (2×10^{-5} mol L^{-1}), using one equivalent of $Cu(ClO_4)_2$ in CH_3CN and a constant temperature of 25 °C. The behaviors of the neutral species **I** (- ·· - ··, measured at 310 nm), the σ-dimer $(\mathbf{I})_2$ (··· ·····, 425 nm), the radical cation $(\mathbf{I})_2^{\bullet+}$ (- - - -, 700 nm), and the dication $(\mathbf{I})_2^{2+}$ (—, 985 nm) are shown.

TABLE 2: The Initial Rates for the Oxidation of I Using Varying Concentrations of Oxidant and Substrate, Measured during the First 3 Seconds at a Constant Temperature of 25 °C

[**I**] (mol L^{-1})	species	[Cu^{2+}] (equivalents)	initial rate[a]
1×10^{-5}	dication	1	1.5×10^{-8}
		3	4.0×10^{-8}
		10	2.2×10^{-7}
	radical cation	1	0.0012
		3	0.0033
	σ-dimer	1	5.9×10^{-9}
		3	1.6×10^{-8}
	neutral	1	-2.3×10^{-8}
		3	-4.3×10^{-8}
		10	-1.8×10^{-7}
2×10^{-5}	dication	1	5.4×10^{-8}
		3	1.8×10^{-7}
		10	5.6×10^{-7}
	radical cation	1	0.0050
		3	0.014
	σ-dimer	1	7.1×10^{-8}
	neutral	1	-9.1×10^{-8}
		3	-4.7×10^{-7}
		10	-5.6×10^{-7}

[a] Units are in mol L^{-1} s^{-1} for all species except the radical cation, which has units of A s^{-1} (absorbance units per second).

$(\mathbf{I})_2^{\bullet+}$ reaction. However, it also seems that $(\mathbf{I})_2^{2+}$ is not a stable species: it reaches an absorbance maximum very early in the oxidation process (<150 s), irrespective of [Cu^{2+}], and begins to decay very quickly. In contrast, the radical cation appears to be more stable: it decays more slowly than the dication and the absorbance maxima consistently occur after that of thedication. This can be seen in the example of 2×10^{-5} mol L^{-1} **I**, shown in Figure 7.

The neutral band at 310 nm decreases very quickly as the sexithiophene charged species form under all conditions trialed for **I**. However, at high [Cu^{2+}], it does not increase again as would be expected for the regeneration of the σ-dimer $(\mathbf{I})_2$ (which absorbs nearby, at 317 nm). This implies that the decay of the charged species at these high oxidant concentrations does not regenerate $(\mathbf{I})_2$ but instead forms unknown degradation products (or higher oligomers). However, when one equivalent of oxidant has been added, the 310-nm band does increase after the initial decay (as shown in Figure 7), suggesting the regeneration of $(\mathbf{I})_2$. Thus, it seems that a low oxidant concentration represents a condition under which regeneration of the neutral from the charged species is possible.

The changes in absorbance over time of the neutral $(\mathbf{I})_2$ peak (measured at 425 nm) show a sharp initial growth which abruptly levels off after two or three minutes, beginning a slower growth that lasts until the end of the experiment. The fast initial increase of $[(\mathbf{I})_2]$, which occurs concurrently with the immediate sharp increases in both $[(\mathbf{I})_2^{\bullet+}]$ and $[(\mathbf{I})_2^{2+}]$, is probably primarily due to a buildup of the $(\mathbf{I})_2$ generated from the extremely rapid σ-dimerization of $\mathbf{I}^{\bullet+}$ before it can be further oxidized. This implies that the $\mathbf{I} \rightarrow \mathbf{I}^{\bullet+} \rightarrow (\mathbf{I})_2$ process is faster than the $(\mathbf{I})_2 \rightarrow (\mathbf{I})_2^{\bullet+}$ reaction. In turn, given the apparent facile nature of the $(\mathbf{I})_2^{\bullet+} \rightarrow (\mathbf{I})_2^{2+}$ process, this suggests that that the $(\mathbf{I})_2 \rightarrow (\mathbf{I})_2^{\bullet+}$ reaction may be the rate-determining step during the oxidation process. The alternative, that this sharp initial increase in $(\mathbf{I})_2$ is due to the reverse $(\mathbf{I})_2^{\bullet+} \rightarrow (\mathbf{I})_2$ reaction, is improbable. At this early stage in the oxidation process, it is unlikely that enough $(\mathbf{I})_2^{\bullet+}$ has accumulated to promote the reverse reaction.

However, the slower increase in $[(\mathbf{I})_2]$ that occurs after the fast initial growth is probably due to the regeneration of $(\mathbf{I})_2$ from its radical cation. This slower increase begins two or three minutes after the reaction begins. At this time, the oxidant has already been consumed, as indicated by the two charged species which reach a concentration maximum at approximately this time (or earlier, as is the case for the dication) and then show a persistent decrease in concentration. In addition, the rate of this slow increase of this 425-nm band matches that of the regeneration of the 310-nm band (close to the second σ-dimer band).

The rate of an electron-transfer reaction is dependent upon the magnitude of the energy barrier (E_a) generated by the intersection of the potential energy surfaces (PESs) of the reactants and products.[37] This is depicted in Figure 8. The energy barrier is determined by the change in energy (ΔE) between the minima of each surface and the reorganization energy (λ), and it is therefore these parameters that dictate the rate. In the generation of an oligothiophene radical cation from its neutral species (or the generation of the dication from a radical cation), the PES of the product is at a higher energy than the reactant. An increase in ΔE (denoting a less stable product) will increase the value of E_a for the forward reaction (e.g. $(\mathbf{I})_2 \rightarrow (\mathbf{I})_2^{\bullet+}$). However, the E_a for the *reverse* reaction (e.g., $(\mathbf{I})_2^{\bullet+} \rightarrow (\mathbf{I})_2$), E_a', will *decrease*. For a given ΔE, an increase in the reorganization energy will lead to an increase in the value of E_a for *both* the forward and reverse reactions. The reorganization energy refers to the required rearrangement of the nuclei from their equilibrium configuration such that the Franck−Condon principle is fulfilled and electron transfer can take place. Thus, a comparison of the kinetic data between the compounds studied may be used to derive information about the relative stabilities of their radical cations and dications.

When one equivalent of oxidant has been added, the initial rates for the decay of the neutral species (measured at 310 nm for **I** and 335 nm for **IV** and **VI**) show that **VI** decays at a slightly faster rate than **IV**, while **I** decays 3−4 times slower (Table 1S). This suggests that the PES for $(\mathbf{I})_2^{\bullet+}$ has a larger ΔE relative to the neutral compound compared to the other two, indicating a less stable radical cation. Both **IV** and **VI** reach

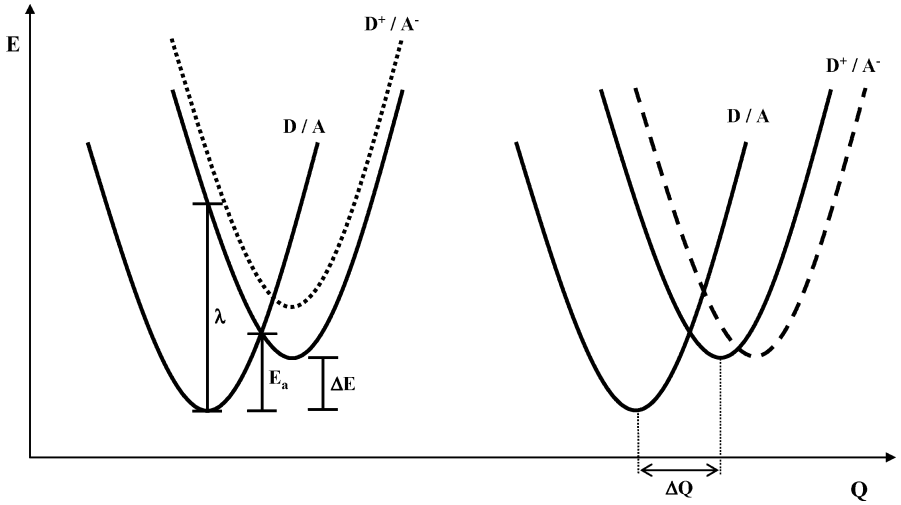

Figure 8. The potential energy surfaces (PESs) for a D/A↔D^+/A^- system (where D refers to the electron donor and A the electron acceptor; for example, D = $\mathbf{I}_2$ and A = Cu^{2+}). The ΔE is the energy difference between the two surfaces' minima. The energy barrier for the reaction is the energy difference between the reactant's PES minimum and the point of intersection between the two surfaces. The E_a shown in the figure refers to the forward reaction D/A→D^+/A^-. The energy barrier of the reverse D^+/A^-→D/A reaction is $E_a' = E_a - \Delta E$. Also shown are the effects of increasing ΔE (left, dotted PES) or, as a result of increasing ΔQ, λ (right, dashed PES) on the energy barriers for both the forward and reverse reactions.

the same minimum concentration (6.5×10^{-6} mol L^{-1}) before regeneration of the neutral species begins. It appears that **IV** regenerates slightly faster than **VI** and at the end of the 90-min experiment, **IV** has achieved a greater regeneration than **VI**. A faster rate for this reverse reaction indicates a smaller E_a' for the reaction and thus a larger ΔE for $\mathbf{IV}^{\bullet+}$. This is supported by the slightly slower initial decay rate for this compound. **I** cannot be inspected in this regard since the regeneration of this band will probably still involve a contribution from the unreacted terthiophene as well as the newly formed sexithiophene. Thus, it seems likely that $\mathbf{IV}^{\bullet+}$ is less stable than $\mathbf{VI}^{\bullet+}$, although their ΔE values are probably very close as the differences in their initial decay rates are relatively small.

Although the extinction coefficients of the radical cations cannot be evaluated, the overall shape of the curve can still be assessed (as this is independent of the value of ϵ). Thus, it can be established that for one equivalent of oxidant added, $(\mathbf{I})_2^{\bullet+}$ decays more quickly than either $\mathbf{IV}^{\bullet+}$ or $\mathbf{VI}^{\bullet+}$. The latter two species have very similar decay curves. Again this suggests that $(\mathbf{I})_2^{\bullet+}$ is the least stable of the radical cations.

The addition of only one equivalent of oxidant shows the appearance of dications for all compounds, indicating the facile nature of this reaction and implying a low E_a for dication formation. However, as was observed for $(\mathbf{I})_2^{2+}$, the dication does not appear to be a stable species and for each compound the absorbance maximum is reached very early in the experiment, prior to 50 s, and the decay occurs very quickly (the decay curves are virtually identical for all dications). This indicates a low E_a' for the reverse reaction as well. In turn, this suggests that the reorganization energy for dication formation is smaller than it is for radical cation generation from the neutral species, as induced by a smaller ΔQ (Figure 8).

The extent of dication formation differs between the compounds. **IV** shows the greatest dication formation (73% of the maximum possible 1×10^{-5} mol L^{-1}) and **I** shows the smallest maximum concentration (28% of the maximum possible 5×10^{-6} mol L^{-1}). The initial rates indicate that $\mathbf{VI}^{2+}$ forms only slightly faster than $\mathbf{IV}^{2+}$ but 7 times faster than $(\mathbf{I})_2^{2+}$ (Table 1S). Given the close similarities between each of the dication decay curves, no conclusions about relative ease of the reverse reactions can be made. These results suggest that $(\mathbf{I})_2^{2+}$ is the least stable dication. $\mathbf{IV}^{2+}$ and $\mathbf{VI}^{2+}$ are difficult to differentiate, suggesting that their PESs are very similar compared to the reactant.

The apparent higher stability of the **IV** and **VI** charged species relative to those of $(\mathbf{I})_2$ will be due to the ability of the electron-donating alkoxy groups to stabilize the positive charges. This was also indicated by the progressive red-shifts observed for the radical cation absorption bands with increasing alkoxy substitution seen in the previous section. This conclusion was supported by ab initio geometry optimizations (B3LYP/6-31G-(d)) done in preparation for the TDDFT study (but without the constraints of C_2 symmetry, vide infra). These calculations show the $(\mathbf{I})_2$ charged species to be higher in energy relative to the neutral state compared to the $(\mathbf{II})_2$ charged species. For instance, $(\mathbf{I})_2^{\bullet+}$ is 3.7 kcal mol^{-1} higher in energy than $(\mathbf{II})_2^{\bullet+}$ (relative to their neutral species, $(\mathbf{I})_2$ and $(\mathbf{II})_2$). In addition, the calculated geometries of the neutral and charged species indicate that a larger structural change is necessary for the transition from the neutral species to the radical cation than for dication formation. In particular, radical cation generation requires a large degree of planarization as well as the expected evolution of a quinoidal bond sequence. In contrast, it appears that no further planarization is necessary during the conversion of a radical cation to a dication and the increasing magnitude of the quinoidal nature of the bond sequence is the only structural change of consequence involved. This observation is consistent with the kinetic data that suggests dication formation has a smaller reorganization energy than radical cation formation, although it must be recalled that the reorganization energy also has a contribution from the solvent.

III.c. Cyclic Voltammetry. The cyclic voltammograms (CVs) of **V** and its σ-dimer, **VI**, are discussed below as representative examples of the series of molecules. The CVs for these two compounds are shown in Figure 9. The other compounds follow the same trends.

The cyclic voltammogram of **V** (Figure 9a) indicates that a coupling process has taken place, consistent with the results observed in section III.a. One anodic peak and two cathodic peaks are seen on the initial scan with three anodic peaks appearing on the second and subsequent scans. The first anodic peak that appears (1.09 V) corresponds to the oxidation of **V**

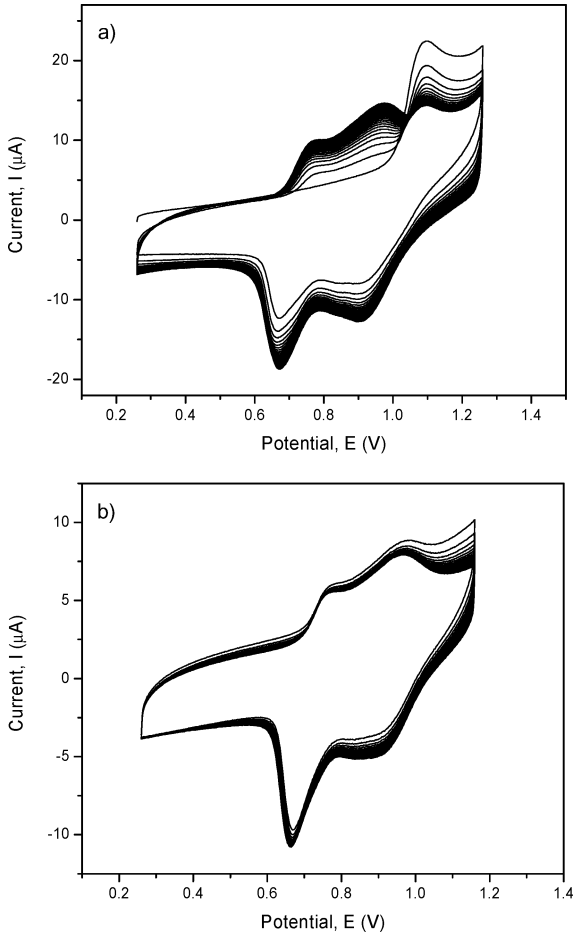

Figure 9. Cyclic voltammograms of 5×10^{-4} mol L^{-1} **V** (a) and 1×10^{-4} mol L^{-1} **VI** (b) in 0.1 mol L^{-1} TBAP/acetonitrile with a scan rate of 10 V s^{-1} (30 scans). Potentials vs SCE and calibrated against $Me_{10}Fc^{+/0}$.

to its radical cation. Fast σ-dimerization to form the sexithiophene occurs and thus the two cathodic peaks at 0.91 and 0.69 V are due to the reduction of the sexithiophene dication to the radical cation and the radical cation to the neutral species, respectively. The following scans then reveal the two new anodic peaks at 0.77 and 0.97 V, corresponding to sexithiophene radical cation and dication formation, respectively. The anodic peak potential for this radical cation formation is less positive than that of the monomer oxidation, as expected for a longer oligothiophene.[38] Similar dimerization behavior has also been observed in the CVs of a thiophene−pyrrole−thiophene oligomer with no α end-caps[39] and short-chain alkyl-substituted oligothiophenes with a single α end-cap.[40] Decreasing the scan rate has the effect of shifting the cathodic peak at 0.91 V to a lower potential (0.84 V). This effect is not concentration dependent and occurs below 5 V s^{-1} for each [**V**] trialed. Therefore, it is likely that this effect is caused by a surface modification of the sexithiophene dication facilitated by this slow time scale. The observation of reversible unsubstituted terthiophene oxidation has only been reported at very high scan rates (15 000 V s^{-1}) in conjunction with the use of ultramicroelectrodes.[39]

To confirm the existence of π-dimers for the compounds studied in this work, CVs were measured at various concentrations of **V**. The dependence of the standard potential E_1° of the $(\mathbf{V})_2/(\mathbf{V})_2^{\bullet+}$ redox couple on the initial concentration c° of **V** shows (Figure 10), within experimental uncertainty, a slope of -29 mV/log(c°). This is in agreement with the theoretical value

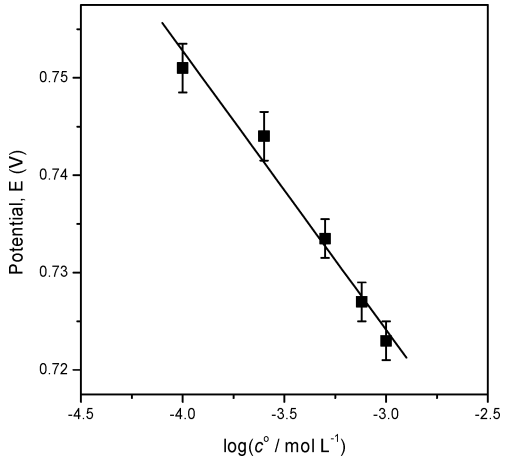

Figure 10. The variation of the standard redox potential E_1° ($(\mathbf{V})_2/(\mathbf{V})_2^{\bullet+}$) with the initial concentration of **V** (log c°) in 0.1 mol L^{-1} TBAP/acetonitrile. Potentials vs SCE and calibrated against $Me_{10}Fc^{+/0}$.

predicted for a fast reversible π-dimer equilibrium at room temperature (298 K) of $-2.3RT/2F = -30$ mV/log(c°).[27,41,42]

Cyclic voltammetry of **VI** (Figure 9b) shows two redox processes, corresponding to the creation of the radical cation and dication. The anodic and cathodic peak potentials are the same as those observed for **V** within experimental uncertainty (standard redox potentials $E_1^\circ = 0.73$ and $E_2^\circ = 0.94$ V), confirming the electronic absorption spectroscopy results that σ-dimerization has indeed occurred for this molecule. These redox potentials, when compared to the higher potentials obtained for unsubstituted sexithiophene in acetonitrile versus the SCE reference ($E_1^\circ = 0.84$ and $E_2^\circ = 1.05$ V),[15] again verify the enhanced stability that the alkoxy-styryl groups impart to the sexithiophene charged species. The CV is reproducible over multiple scans, showing only small current increases; thus, the oxidized species are stable and no further oligomerization is taking place. Altering the scan rate has no effect on the overall shape of the CV.

III.d. TDDFT Calculations. The electronic excitation energies of the simplest σ-dimers $(\mathbf{I})_2$ and $(\mathbf{II})_2$ and their radical cations and dications were calculated using time-dependent DFT (TDDFT) with the B3LYP/6-31G(d) method. We found this to be the maximum basis set size possible for these systems; even so, it was required that C_2 symmetry be imposed to reduce the computational cost. To provide a means of comparison with the $(\mathbf{I})_2$ and $(\mathbf{II})_2$ systems, TDDFT calculations were first performed on unsubstituted sexithiophene, 6T, and its radical cation $6T^{\bullet+}$ and dication $6T^{2+}$, also using the method B3LYP/6-31G(d). All calculated electronic excitation energies, oscillator strengths, and CI coefficients are presented in Table 3.

Neutral 6T is predicted to have an intense band at 2.45 eV, assigned to the HOMO→LUMO transition, with an oscillator strength of $f = 1.96$. Experimentally, a single broad band is observed at 2.86 eV.[5] The deviation of the calculated transition energy from this measured value, although high at 0.41 eV, is not without precedent. TDDFT calculations have in the past shown large deviations between experimental and calculated transition energies of 0.4−0.7 eV for neutral[43] and charged[44] species of conjugated systems. Previous excitation energy calculations on neutral unsubstituted sexithiophene have produced similar results.[45−47] For example, a TDDFT calculation on this species using the B3LYP/6-311G(d,p) method predicted the transition at 2.57 eV, $f = 1.89$.[48] A less intense transition has also been calculated at 3.67 eV ($f = 0.25$), which is not evident in the experimental absorption spectrum, probably

TABLE 3: Vertical Transition Energies and Oscillator Strengths (f) Calculated Using TDDFT with the Method B3LYP/6-31G(d) and Compared to Experimental Data[a]

molecule	experimental transition energy[a]		calculated transition energy	oscillator strength	transition	CI coefficient
6T	2.86		2.45	1.96	HOMO→LUMO	0.64
			3.67	0.25	HOMO-1→LUMO+1	0.61
					HOMO-2→LUMO	0.32
$6T^{\bullet+}$	0.84		0.94	0.43	HOMO-1→SOMO	0.83
	1.59		1.79	1.83	SOMO→LUMO	0.83
$6T^{2+}$	1.24		1.58	2.61	HOMO→LUMO	0.49
$(\mathbf{I})_2$	2.83		2.33	1.38	HOMO→LUMO	0.66
	3.91		3.37	0.53	HOMO-2→LUMO	0.47
					HOMO→LUMO+3	0.40
					HOMO-1→LUMO+1	−0.28
$(\mathbf{I})_2^{\bullet+}$	0.85		0.90	0.37	HOMO-1→SOMO	0.86
			1.36	0.11	HOMO-3→SOMO	0.94
	1.54		1.63	1.39	SOMO→LUMO	0.86
$(\mathbf{I})_2^{2+}$	1.26[b]		1.29	0.83	HOMO→LUMO	0.46
					HOMO-2→LUMO	0.37
	1.39[b]	1.26[b]	1.57	1.41	HOMO-2→LUMO	0.50
					HOMO→LUMO	−0.28
$(\mathbf{II})_2$	2.85		2.29	1.38	HOMO→LUMO	0.65
	3.80		3.28	0.52	HOMO→LUMO+3	0.56
					HOMO-1→LUMO+1	−0.28
					HOMO-2→LUMO	0.26
$(\mathbf{II})_2^{\bullet+}$	0.81		0.82	0.35	HOMO-1→SOMO	0.87
			1.23	0.17	HOMO-3→SOMO	0.92
	1.52		1.58	1.27	SOMO→LUMO	0.86
$(\mathbf{II})_2^{2+}$	1.28[b]		1.17	0.88	HOMO→LUMO	0.53
					HOMO-2→LUMO	0.21
	1.39[b]	1.28[b]	1.52	1.23	HOMO-2→LUMO	0.56
					HOMO→LUMO	−0.13
	2.36		2.29	0.41	HOMO-1→LUMO+1	0.49
					HOMO-4→LUMO	−0.45

[a] Experimental transition energies for 6T, $6T^{\bullet+}$, and $6T^{2+}$ are from refs 5 and 15; all others are converted from Table 1 in this work. [b] Both assignment possibilities are presented for the dications. [c] Transition energies are in electronvolts (eV).

because of the large intensity and breadth of the observable band. The CI coefficients indicate that this is a mixed transition, with contributions from the HOMO-2→LUMO and HOMO-1→LUMO+1 configurations.

Two electronic transitions are calculated for $6T^{\bullet+}$ at 0.94 eV ($f = 0.43$) and 1.79 eV ($f = 1.83$). The former is primarily due to a transition between the doubly occupied HOMO-1 and the singly occupied MO (SOMO) while the latter is due to the SOMO→LUMO transition, assignments consistent with those stated in the literature.[5,34] The measured electronic absorption spectrum of $6T^{\bullet+}$ displays two strong bands at 0.84 and 1.59 eV,[15] which correlate well with the predicted transitions.

The absorption spectrum of $6T^{2+}$ is predicted to show a single very intense band at 1.58 eV ($f = 2.61$) and this is also observed experimentally, with the single band appearing at 1.24 eV.[5,11] The calculated band is assigned to the HOMO→LUMO transition.

TDDFT calculations using the B3LYP/6-31G(d) method were also performed on $(\mathbf{I})_2$ and its radical cation and dication. The excitation energies calculated for $(\mathbf{I})_2$ show two strong transitions at 2.33 eV ($f = 1.38$) and 3.37 eV ($f = 0.53$). The lower energy band is assigned to the HOMO→LUMO excitation (slightly red-shifted compared to the corresponding band in 6T) while the 3.37 eV band contains significant contributions from several configurations, notably the HOMO-2→LUMO, HOMO→LUMO+3, and HOMO-1→LUMO+1 excitations. Examination of the calculated MOs of neutral $(\mathbf{I})_2$ (Figure 6S) has revealed that the HOMO-2 and LUMO+3 are localized primarily on the styryl substituents. It is therefore probable that it is the presence of these new styryl-based MOs that cause a second band to be observed experimentally, in contrast to the single band observed for 6T. The two experimental bands of $(\mathbf{I})_2$ are measured at 2.83 (438 nm) and 3.91 eV (317 nm): the TDDFT calculation has consistently underestimated both transition energies of $(\mathbf{I})_2$ by about 0.5 eV.

Two strong electronic transitions are predicted for $(\mathbf{I})_2^{\bullet+}$ at 0.90 eV ($f = 0.37$) and 1.63 eV ($f = 1.39$). As was the case with $6T^{\bullet+}$ and other TDDFT oligothiophene calculations,[25] the lower energy transition is primarily due to the HOMO-1→SOMO excitation and the higher energy transition is mostly due to the SOMO→LUMO excitation. These MOs are shown in Figure 7S. In addition, a weaker band is also predicted at 1.36 eV ($f = 0.11$) and is caused by the HOMO-3→SOMO transition. The HOMO-3 possesses significant orbital density on the styryl groups (and terminal thiophene rings), explaining why no such transition is predicted for $6T^{\bullet+}$. This weak transition is not evident in the experimental spectrum and it is likely that it is being obscured by the two observed transitions of greater intensity. These two measured bands, at 0.85 eV (1466 nm) and 1.54 V (806 nm), are both within 0.1 eV of the calculated transitions, indicating a good agreement. The theoretical prediction of three transitions while two bands are observed experimentally has also been seen for the terthiophene radical cation, calculated using the CASPT2 method by Rubio et al:[49] the high-energy band measured at 2.25 eV has been proposed to be caused by two electronic transitions.

As with $(\mathbf{I})_2^{\bullet+}$, the calculated excitation energies of $(\mathbf{I})_2^{2+}$ show an additional band that is not predicted for unsubstituted sexithiophene. Two strong bands are predicted for $(\mathbf{I})_2^{2+}$ at 1.29 eV ($f = 0.83$) and 1.57 eV ($f = 1.41$). Each transition has a significant contribution from both the HOMO-2→LUMO and HOMO→LUMO configurations (although the 1.57 eV band has a CI coefficient for the HOMO-2→LUMO excitation twice that of the HOMO−LUMO excitation). The HOMO-2 orbital is primarily styryl-based. The pertinent MOs for these transitions are depicted in Figure 11. Experimentally, one very intense band

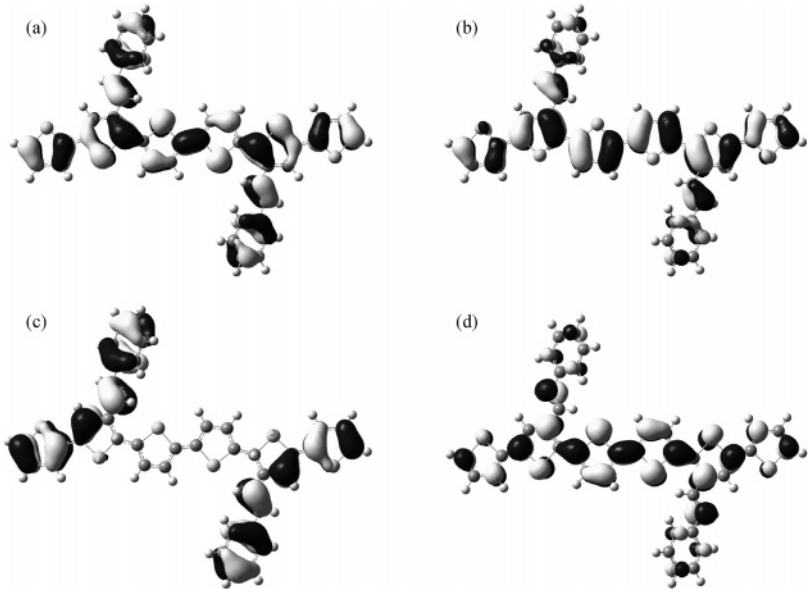

Figure 11. Molecular orbitals of $(\mathbf{I})_2^{2+}$, calculated using the B3LYP/6-31G/d method; the HOMO (reproduced in Figure 12) (a), LUMO (b), HOMO-2 (c), and LUMO+1 (d) are shown.

at 1.26 eV (984 nm) and a well-defined shoulder at 1.39 eV (890 nm) is observed for $(\mathbf{I})_2^{2+}$. The shape and wavelengths of both the main band and the shoulder are very similar to that observed for $6T^{2+}$. The main band of $6T^{2+}$ (1.24 eV) has been assigned to the HOMO→LUMO transition while the shoulder (1.36 eV) is generally attributed to vibronic coupling.[19] If this $6T^{2+}$ assignment were extrapolated to the $(\mathbf{I})_2^{2+}$ system, then the measured band at 1.26 eV (correlated with the measured $6T^{2+}$ band at 1.24 eV) would therefore be assigned to the calculated 1.57 eV band (1.58 eV for $6T^{2+}$). However, although the wavelengths of the two bands match very well, the configurations involved in the transition do not: the 1.57 eV band of $(\mathbf{I})_2^{2+}$, as mentioned above, contains a much higher contribution from the HOMO-2→LUMO excitation than the HOMO→LUMO excitation, while the corresponding transition of $6T^{2+}$ is solely HOMO→LUMO. This alone suggests that the similarities between the two measured spectra may be a coincidence. In addition, this assignment implies that the second $(\mathbf{I})_2^{2+}$ predicted band (1.29 eV), although of appreciable oscillator strength, is not evident in the measured spectrum at all.

An alternative assignment involves attributing the calculated bands 1.29 and 1.57 eV to the main band measured at 1.26 eV and the shoulder at 1.39 V, respectively. If this assignment is correct, then it does provide a good agreement between the transition energies (however, the oscillator strengths have been miscalculated). Therefore, the main bands in the measured spectrum of $(\mathbf{I})_2^{2+}$ and $6T^{2+}$ both contain a contribution from the HOMO→LUMO configuration (although the $(\mathbf{I})_2^{2+}$ band also involves a sizable contribution from the HOMO-2→LUMO excitation). The shoulder, however, has a different origin for the two species: vibronic coupling in $6T^{2+}$ and a primarily HOMO-2→LUMO transition for $(\mathbf{I})_2^{2+}$.

Despite the uncertainty involved in assigning the $(\mathbf{I})_2^{2+}$ transitions and regardless of which assignment is more probable, it seems reasonable to conclude from the TDDFT results that the main band observed at 984 nm has significant HOMO-2→LUMO character in addition to the HOMO→LUMO excitation. The similarities between the two measured dication absorption spectra of $6T^{2+}$ and $(\mathbf{I})_2^{2+}$ may arise from the fact

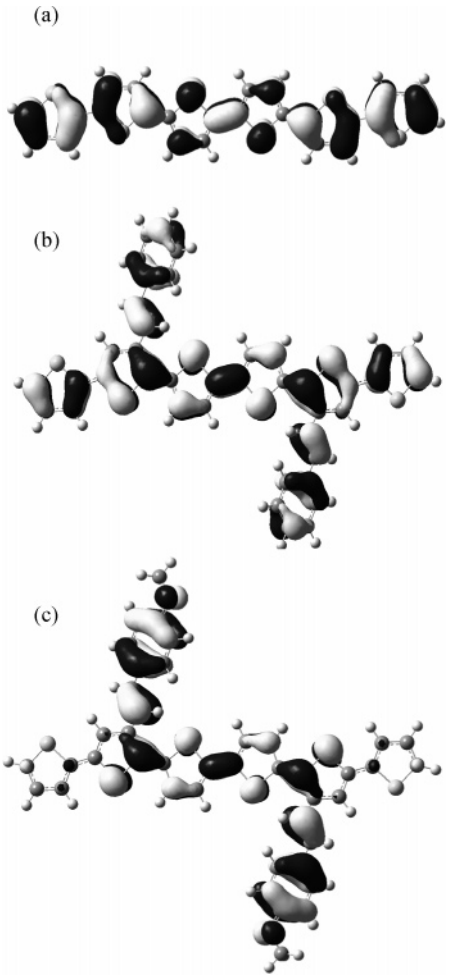

Figure 12. HOMOs of $6T^{2+}$, $(\mathbf{I})_2^{2+}$, and $(\mathbf{II})_2^{2+}$, calculated using the B3LYP/6-31G(d) method.

that the HOMO and LUMO for both species have a very similar thiophene backbone orbital arrangement (Figure 12).

TDDFT calculations were also carried out on $(\mathbf{II})_2$ and its charged derivatives using C_2 symmetry and the B3LYP/6-31G-(d) method. Very similar results to $(\mathbf{I})_2$ and its radical cation

and dication were found, although the transition energies were red-shifted (as expected because of the higher stability of the charged species of $(\mathbf{II})_2$). In particular, the transition energies for $(\mathbf{II})_2^{2+}$ were 1.17 eV ($f = 0.88$) and 1.52 eV ($f = 1.23$) and were due to the same excitations as observed for $(\mathbf{I})_2^{2+}$. The oscillator strengths of the two predicted bands are more equivalent for this species than for $(\mathbf{I})_2^{2+}$. The experimental spectrum of $(\mathbf{II})_2^{2+}$ shows a broad band at 1.39 eV (889 nm) and a shoulder at 1.28 eV (965 nm) with almost equivalent intensity. The relative intensities and band energies are thus more consistent with the second assignment possibility stated above, that is, the predicted bands at 1.17 and 1.52 eV correspond to the measured 1.28 eV shoulder and 1.39 eV band, respectively. However, given the broadness of the principal band, the first assignment possibility cannot be ruled out. In addition, the HOMO of $(\mathbf{II})_2^{2+}$ has notably less thiophene backbone character than the corresponding MO of $6T^{2+}$ or $(\mathbf{I})_2^{2+}$, as shown in Figure 12. This may be contributing to the different dication band structure observed experimentally for $(\mathbf{II})_2^{2+}$.

The $(\mathbf{II})_2^{2+}$ TDDFT calculation also predicts a higher energy band at 2.29 eV ($f = 0.41$) that is assigned to the experimentally observed 2.36 eV (527 nm) band. This is a mixed transition, with contributions from the HOMO-1→LUMO+1 and HOMO-4→LUMO excitations.

IV. Conclusions

The electronic absorption spectra of the chemical oxidations of compounds **I**−**VI** using $Cu(ClO_4)_2/CH_3CN$ reveal very similar behavior. The terthiophenes all σ-dimerize to form sexithiophenes, which then undergo further oxidation. There is clear evidence of sexithiophene radical cations, dications, and π-dimers in the absorption spectra. In general, the two radical cation bands appear at 1465−1580 and 805−825 nm while the blue-shifted π-dimer bands are measured at 1170−1225 and 695−750 nm. The presence of π-dimer bands in these spectra is not surprising: both the oligothiophene length and the use of acetonitrile favor π-dimers, and these bands dominate the early oxidation stage of compounds **II**−**VI**. The oxidation of more concentrated solutions produces primarily π-dimer bands. **I** appears to show the least tendency to π-dimerize.

The two sexithiophenes, **IV** and **VI**, were also oxidized using $FeCl_3/CH_2Cl_2$. Only radical cation bands were observed for **IV**, whereas in the **VI** π-dimer bands followed the initial radical cation formation. Dication formation did not occur for either compound in this solvent.

Both the radical cation and π-dimer bands show a red-shift across the molecule series as the extent of the alkoxy substitution increases. This can be attributed to the electron-donating alkoxy groups, which are conjugated to the rest of the π-system, stabilizing the radical cation. Conversely, the position of the main dication band does not shift with increasing substitution and remains at approximately the same wavelength (885−895 nm). However, the structure of the dimer dication band does vary between the different compounds. In **I**, the band at 984 nm is the most intense with the 890-nm transition as a shoulder. In contrast, the intensities of the corresponding bands for **II** are reversed, while for the remaining compounds the ∼980-nm transition is not visible at all and the 890-nm transition dominates the spectrum.

Kinetic analyses have verified the increased stability of those compounds with alkoxy substituents and indicate that the sexithiophene radical cation and dication formation reactions are third-order overall. No evidence of terthiophene charged species are observed, even within the first few seconds, and regeneration of the neutral sexithiophenes were observed under low oxidant conditions.

Cyclic voltammetry has confirmed both the σ-dimerization process and the presence of a reversible π-dimer equilibrium at room temperature. It has also confirmed the enhanced stability of the alkoxy-styryl sexithiophene charged species relative to those of unsubstituted sexithiophene.

TDDFT calculations successfully predicted the presence of two bands in the electronic absorption spectra of neutral $(\mathbf{I})_2$ and $(\mathbf{II})_2$. The second band, which is not observed for neutral unsubstituted sexithiophene, has strong contributions from excitations involving styryl-based MOs. The radical cation absorption spectra were also well predicted. $(\mathbf{I})_2^{2+}$, however, is predicted to have two intense bands and the correlation with the experimental spectrum is ambiguous. Nevertheless, it can be concluded that the HOMO-2, an orbital localized primarily on the styryl substituents, plays a significant role in the dication transitions. In $(\mathbf{II})_2^{2+}$, for which the measured dication band has a very different appearance to that of $(\mathbf{I})_2^{2+}$, it seems more feasible to assign the broad principal band and its shoulder to the two calculated transitions. The HOMO of $(\mathbf{II})_2^{2+}$ has appreciably less orbital density on the thiophene backbone than is observed for $6T^{2+}$ and $(\mathbf{I})_2^{2+}$. Indeed, the thiophene backbones of $6T^{2+}$ and $(\mathbf{I})_2^{2+}$ display a very similar HOMO (and LUMO) structure. This could be contributing to the similarities between the electronic absorption spectra of $6T^{2+}$ and $(\mathbf{I})_2^{2+}$ and the change in the band maximum and shape when an alkoxy group is introduced.

Both the styryl and alkoxy groups are clearly having a significant effect on the electronic properties of this class of molecules.

Through careful control of substrate concentration, it is possible to examine the interplay between π-dimer formation and radical cation and dication formation in these compounds. The prevalence of π-dimers in what are comparatively dilute solutions suggests that these interactions may be extremely important with regard to the electronic properties of solid-state devices.

Acknowledgment. The authors are grateful to the New Zealand Foundation of Science, Research, and Technology and the University of Otago for support.

Supporting Information Available: The electronic absorption spectra of the chemical oxidation of 10^{-4} mol L^{-1} **II** (Figure 1S), 10^{-5} and 10^{-4} mol L^{-1} **III** (Figures 2S and 3S, respectively), 10^{-5} and 10^{-4} mol L^{-1} **IV** (Figures 4S and 5S, respectively), selected kinetic data of **I**, **IV**, and **VI** (Table 1S), and selected calculated molecular orbitals of $(\mathbf{I})_2$ and $(\mathbf{I})_2^{\bullet+}$ (Figures 6S and 7S, respectively). This material is available free of charge via the Internet at http://pubs.acs.org.

References and Notes

(1) (a) Katz, H. E. *J. Mater. Chem.* **1997**, *7*, 369. (b) Horowitz, G. *Adv. Mater.* **1998**, *10* (5), 365.

(2) (a) Burroughes, J. H.; Bradley, D. D. C.; Brown, A. R.; Marks, R. N.; Mackay, K.; Friend, R. H.; Burns, P. L.; Holmes, A. B. *Nature* **1990**, *347*, 539. (b) Dai, L.; Winkler, B.; Dong, L.; Tong, L.; Mau, A. W. H. *Adv. Mater.* **2001**, *13*, 915.

(3) Pron, A.; Rannou, P. *Prog. Polym. Sci.* **2002**, *27*, 135.

(4) Gazotti, W. A.; Nogueira, A. F.; Girotto, E. M.; Micaroni, L.; Martini, M.; das Neves, S.; De Paoli, M.-A. In *Handbook of Advanced Electronic and Photonic Materials and Devices*; Nalwa, H. S., Ed; Academic Press: San Diego, CA, 2001.

(5) Furukawa, Y. *J. Phys. Chem.* **1996**, *100*, 15644.

(6) Gao, Y.; Liu, C.; Jiang, Y. *J. Phys. Chem. A* **2002**, *106*, 5380.

(7) Apperloo, J. J.; Janssen, R. A. J.; Malenfant, P. R. L.; Groenendaal, L.; Fréchet, J. M. J. *J. Am. Chem. Soc.* **2000**, *122*, 7042.
(8) Irle, S.; Lischka, H. *J. Chem. Phys.* **1997**, *107* (8), 3021.
(9) van Haare, J. A. E. H.; Havinga, E. E.; van Dongen, J. L. J.; Janssen, R. A. J. Cornil, J.; Brédas, J.-L. *Chem. Eur. J.* **1998**, *4* (8), 1509.
(10) Hill, M. G.; Mann, K. R.; Miller, L. L.; Penneau, J. *J. Am. Chem. Soc.* **1992**, *114* (7), 2728.
(11) Wintgens, V.; Valat, P.; Garnier, F. *J. Phys. Chem.* **1994**, *98* (1), 228.
(12) Helbig, M.; Hein, J.; Rentsch, S.; Bürger, H.; Hobert, H. *Chem. Phys.* **1998**, *227*, 111.
(13) Evans, C. H.; Scaiano, J. C. *J. Am. Chem. Soc.* **1990**, *112* (7), 2694.
(14) Emmi, S. S.; D'Angelantonio, M.; Beggiato, G.; Poggi, G.; Geri, A.; Pietropaolo, D.; Zotti, G. *Radiat. Phys. Chem.* **1999**, *54*, 263.
(15) Fichou, D.; Horowitz, G.; Xu, B.; Garnier, F. *Synth. Met.* **1990**, *39*, 243.
(16) Kankare, J.; Lukkari, J.; Pasanen, P.; Sillanpää, R.; Laine, H.; Harmaa, K. *Macromolecules* **1994**, *27*, 4327.
(17) Bäuerle, P.; Segelbacher, U.; Maier, A.; Mehring, M. *J. Am. Chem. Soc.* **1993**, *115*, 10217.
(18) Guay, J.; Kasai, P.; Diaz, A.; Wu, R.; Tour, J. M.; Dao, L. H. *Chem. Mater.* **1992**, *4*, 1097.
(19) Zinger, B.; Mann, K. R.; Hill, M. G.; Miller, L. L. *Chem. Mater.* **1992**, *4*, 1113.
(20) Yu, Y.; Gunic, E.; Zinger, B.; Miller, L. L. *J. Am. Chem. Soc.* **1996**, *118*, 1013.
(21) Yokonuma, N.; Furukawa, Y.; Tasumi, M.; Kuroda, M.; Nakayama, J. *Chem. Phys. Lett.* **1996**, *255*, 431.
(22) Helbig, M.; Ruseckas, A.; Grage, M. M.-L.; Birckner, E.; Rentsch, S.; Sundström. *Chem. Phys. Lett.* **1999**, *302*, 587.
(23) Hill, M. G.; Penneau, J.; Zinger, B.; Mann, K. R.; Miller, L. L. *Chem. Mater.* **1992**, *4*, 1106.
(24) Graf, D. D.; Duan, R. G.; Campbell, J. P.; Miller, L. L.; Mann, K. R. *J. Am. Chem. Soc.* **1997**, *119* (25), 5888.
(25) Alberti, A.; Ballarin, B.; Guerra, M.; Macciantelli, D.; Mucci, A.; Parenti, F.; Schenetti, L.; Seebar, R.; Zanardi, C. *Chem. Phys. Chem.* **2003**, *4*, 1216.
(26) Nessakh, B.; Horowitz, G.; Garnier, F.; Deloffre, F.; Srivastava, P.; Yassar, A. *J. Electroanal. Chem.* **1995**, *399*, 97.
(27) Levillain, E.; Roncali, J. *J. Am. Chem. Soc.* **1999**, *121*, 8760.
(28) Apperloo, J. J.; Groenendaal, L.; Verheyen, H.; Jayakannan, M.; Janssen, R. A. J.; Dkhissi, A.; Beljonne, D.; Lazzaroni, R.; Brédas, J.-L. *Chem. Eur. J.* **2002**, *8* (10), 2384.
(29) Collis, G. E.; Burrell, A. K.; Scott, S. M.; Officer, D. L. *J. Org. Chem.* **2003**, *68* (23), 8974.
(30) Grant, D. K.; Officer, D. L. In preparation.
(31) Noviandri, I.; Brown, K. N.; Fleming, D. S.; Gulyas, P. T.; Lay, P. A.; Masters, A. F.; Phillips, L. *J. Phys. Chem. B* **1999**, *103*, 6713.
(32) Frisch, M. J.; Trucks, G. W.; Schlegel, H. B.; Scuseria, G. E.; Robb, M. A.; Cheeseman, J. R.; Montgomery, J. A., Jr.; Vreven, T.; Kudin, K. N.; Burant, J. C.; Millam, J. M.; Iyengar, S. S.; Tomasi, J.; Barone, V.; Mennucci, B.; Cossi, M.; Scalmani, G.; Rega, N.; Petersson, G. A.; Nakatsuji, H.; Hada, M.; Ehara, M.; Toyota, K.; Fukuda, R.; Hasegawa, J.; Ishida, M.; Nakajima, T.; Honda, Y.; Kitao, O.; Nakai, H.; Klene, M.; Li, X.; Knox, J. E.; Hratchian, H. P.; Cross, J. B.; Adamo, C.; Jaramillo, J.; Gomperts, R.; Stratmann, R. E.; Yazyev, O.; Austin, A. J.; Cammi, R.; Pomelli, C.; Ochterski, J. W.; Ayala, P. Y.; Morokuma, K.; Voth, G. A.; Salvador, P.; Dannenberg, J. J.; Zakrzewski, V. G.; Dapprich, S.; Daniels, A. D.; Strain, M. C.; Farkas, O.; Malick, D. K.; Rabuck, A. D.; Raghavachari, K.; Foresman, J. B.; Ortiz, J. V.; Cui, Q.; Baboul, A. G.; Clifford, S.; Cioslowski, J.; Stefanov, B. B.; Liu, G.; Liashenko, A.; Piskorz, P.; Komaromi, I.; Martin, R. L.; Fox, D. J.; Keith, T.; Al-Laham, M. A.; Peng, C. Y.; Nanayakkara, A.; Challacombe, M.; Gill, P. M. W.; Johnson, B.; Chen, W.; Wong, M. W.; Gonzalez, C.; Pople, J. A. *Gaussian 03*, Revision B.04; Gaussian, Inc.: Pittsburgh, PA, 2003.
(33) Clarke, T. M.; Gordon, K. C.; Officer, D. L.; Hall, S. B.; Collis, G. E.; Burrell, A. K. *J. Phys. Chem. A* **2003**, *107*, 11505.
(34) Casado, J.; Ruiz Delgado, M. C.; Shirota, Y.; Hernández, V.; López Navarrete, J. T. *J. Phys. Chem. B* **2003**, *107*, 2637.
(35) Horowitz, G.; Yassar, A.; Von Bardeleben, H. J. *Synth. Met.* **1994**, *62* (3), 245.
(36) DFT calculations have provided an explanation for the observation of the head-to-head (HH) sexithiophene regioisomer, as opposed to the other two possibilities (head-to-tail and tail-to-tail), when two terthiophene radical cations couple together. A geometry optimization of the terthiophene radical cation $\mathbf{V}^{\bullet+}$ (the long-chain alkoxy substituent on the phenyl ring was modeled by halving its length) using the B3LYP/6-31G(d) method has revealed that the spin density on the terminal α carbon of the "head" thiophene ring is almost twice that of the corresponding carbon of the "tail" thiophene ring. This is common for the radical cations of all the terthiophenes studied in this work and will be discussed in further detail in another paper.[30] It has been well established that a coupling reaction between two oligothiophene radical cations preferentially occurs between the two terminal α carbons having the highest spin densities.[50] In the species examined in this work, the "head" α carbon of the terthiophene radical cation is thus more reactive and σ-dimerization between two of these centers will result in the HH sexithiophene isomer.
(37) *Progress in Inorganic Chemistry*; Lippard, S. J., Ed.; John Wiley and Sons: Cambridge, MA, 1983; Vol. 30.
(38) Cutler, C. A.; Burrell, A. K.; Collis, G. E.; Dastoor, P. C.; Officer, D. L.; Too, C. O.; Wallace, G. G. *Synth. Met.* **2001**, *123*, 225.
(39) Audebert, P.; Catel, J.-M.; Le Coustumer, G.; Duchenet, V.; Hapiot, P. *J. Phys. Chem. B* **1998**, *102*, 8661.
(40) Barth, M.; Guilerez, S.; Bidan, G.; Bras, G.; Łapkowski, M. *Electrochim. Acta* **2000**, *45*, 4409.
(41) Hapiot, P.; Gaillon, L.; Audebert, P.; Moreau, J. J. E.; Lére-Porte, J.-P.; Wong Chi Man, M. *J. Electroanal. Chem.* **1997**, *435*, 85.
(42) Hapiot, P.; Audebert, P.; Monnier, K.; Pernaut, J.-M.; Garcia, P. Electrochemical evidence of π-dimerisation with short thiophene oligomers. *Chem. Mater.* **1994**, *6*, 1549.
(43) Hsu, C.; Hirata, S.; Head-Gordon, M. *J. Phys. Chem. A* **2001**, *105*, 451.
(44) Pou-Amérigo, R.; Viruela, P. M.; Viruela, R.; Rubio, M.; Ortí, E. *Chem. Phys. Lett.* **2002**, *352*, 491.
(45) Beljonne, D.; Cornil, J.; Friend, R. H.; Janssen, R. A. J.; Brédas, J. L. *J. Am. Chem. Soc.* **1996**, *118*, 6453.
(46) Colditz, R.; Grebner, D.; Helbig, M.; Rentsch, S. *Chem. Phys.* **1995**, *201*, 309.
(47) Cornil, J.; Brédas, J. L. *Adv. Mater.* **1995**, *7* (3), 295.
(48) Pogantsch, A.; Heimel, G.; Zojer, E. *J. Chem. Phys.* **2002**, *117* (12), 5921.
(49) Rubio, M.; Ortí, E.; Pou-Amérigo, R.; Merchán, M. *J. Phys. Chem.* **2001**, *105*, 9788.
(50) Ando, S.; Ueda, M. *Synth. Met.* **2002**, *129*, 207.